Simulations of the formation of thick discs in galaxies

Villalobos Cofre, Alvaro Andres

Chapter 3

Simulations of minor mergers. II. The phase-space structure of thick discs*

Abstract

We analyse the phase-space structure of simulated thick discs that are the result of a significant merger between a disc galaxy and a satellite. Our main goal is to establish what would be the characteristic imprints of a merger origin for the Galactic thick disc. We find that the spatial distribution predicted for thick disc stars is asymmetric, seemingly in agreement with recent observations of the Milky Way thick disc. Near the Sun, the accreted stars are expected to rotate more slowly, to have broad velocity distributions, and to occupy preferentially the wings of the line-of-sight velocity distributions. The majority of the stars in our model thick discs have low eccentricity orbits (in clear reference to the pre-existing heated disc) which gives rise to a characteristic (sinusoidal) pattern for their line of sight velocities as function of galactic longitude. The z-component of the angular momentum of thick disc stars provides a clear discriminant between stars from the pre-existing disc and those from the satellite, particularly at large radii. These results are robust against the particular choices of initial conditions made in our simulations, and thus provide clean tests of the disc heating via a minor merger scenario for the formation of thick discs.

* Based on Villalobos & Helmi 2009, submitted to MNRAS on February 8th, 2009

3.1 Introduction

Thick discs appear to be a common feature of disc galaxies (Yoachim & Dalcanton 2006, and references therein). They are believed to be snap-frozen relics of disc galaxy formation that took place at high-redshift (Freeman & Bland-Hawthorn 2002). This is because their dominant stellar populations appear to be old, as indicated for example by the colours of the envelopes of edge-on disc galaxies (see, e.g. Dalcanton & Bernstein 2002, and follow-up papers). More direct evidence comes from local studies of the Milky Way's thick disc, whose stars are mostly older than 10–12 Gyr (e.g. Edvardsson et al. 1993).

In the case of the Milky Way, the thick disc has structural, kinematic and chemical properties that in general are significantly different compared to the other Galactic components (Bensby et al. 2005; Jurić et al. 2008; Veltz et al. 2008). This implies that it is quite likely it has followed its independent evolutionary path, as discussed in Wyse (2004) and references therein (but see also Ivezić et al. 2008).

As stated above, the Galactic thick disc provides us with a window into the high-redshift Universe. However unlike the Galactic stellar halo, which is also ancient, the thick disc contains a non-negligible fraction of the total stellar mass of the Galaxy (between 6 and 15 per cent, e.g. Robin et al. 2003; Jurić et al. 2008), what enhances its importance as a tracer of the events that took place at early epochs. On the other hand, and like for the stellar halo, imprints of that early history may be present in the form of dynamical or chemical substructure. This information could, in principle, be retrieved relatively easily from large surveys of nearby stars implying that we can hope to directly test the various scenarios proposed for its formation.

These various scenarios may be classified according to the relative importance of dissipative processes. The collapse of a gas cloud with a large scale-height (Eggen et al. 1962; Burkert et al. 1992), or intense star formation (Kroupa 2002), perhaps triggered by gas rich mergers (Brook et al. 2004; Bournaud et al. 2007a) are two dissipationally driven models. On the other hand, the vertical heating of a thin disc during a merger event (e.g. Kazantzidis et al. 2008, and references therein); or the direct accretion of satellites proposed by Abadi et al. (2003) are examples of (mostly) dissipationless processes.

In the case of a merger origin of the Galactic thick disc, one may expect significant substructure to be present, particularly in the phase-space distribution of its stars. In fact, evidence of such merger debris in our Galaxy has been mounting over the past decade. Examples are the substantial group of stars located a few kpc from the Galactic plane with kinematics intermediate between the canonical thick disc and the canonical stellar halo (Gilmore et al. 2002b); or the significant asymmetry in the distribution of thick disc stars in the first Galactic quadrant with respect to the fourth (Parker et al. 2003, 2004; Larsen et al. 2008). In addition to substructure of the thin/thick disc such as the Arcturus stream (Eggen 1996; Navarro et al. 2004), the Monoceros ring (Yanny et al. 2003), the Canis Major dwarf (Martin et al. 2004), distinctive stellar groups in the solar vicinity with peculiar ages, metallicities and kinematics have also been discovered (Helmi et al. 2006). All these observations thus appear to support models in which the thick disc was formed by accretion and/or merger events.

In Villalobos & Helmi (2008, hereafter, Chapter 2) we presented a series of simulations of minor mergers between a disc galaxy and a relatively massive satellite, with the aim of modelling the formation of a thick disc (a scenario first explored thoroughly by Quinn

et al. 1993, and which has received much attention since then). The present work is intended as a follow-up study where we particularly focus on characterising the phase-space properties of these simulated thick discs. Our ultimate goal is to find sets of observables that would allow us to recover traces of the merger that may have lead to the formation of the Galactic thick disc. In principle, it should also be possible to distinguish stars from the intruder satellite from those of the heated disc in the final aftermath.

We are also motivated to pursue such a study at this point in time by the surveys that are currently mapping the Milky Way galaxy and its components in great detail. In particular, the spectroscopic RAVE and SEGUE/SDSS surveys are both providing large samples of stars with accurate kinematics (Zwitter et al. 2008; Adelman-McCarthy et al. 2008; Lee et al. 2008). Such surveys will enable a more precise characterisation of the Galactic thick disc, and should allow us to test the various formation scenarios discussed above. On a slightly longer timescale, the space astrometric mission *Gaia* will provide full phase-space coordinates for hundreds of millions of stars (Perryman et al. 2001), from which we should be able to establish how the Galactic thick disc was assembled.

The outline of this Chapter is the following. In Section 2 we briefly describe the numerical simulations that are used in this study. In Section 3 we characterise the velocity distribution in local volumes resembling the Solar neighbourhood. In this section we put special emphasis on understanding the predicted distributions of heliocentric line-of-sight velocities since, in practice, these can be obtained with high accuracy for large samples of stars, and are available even at the present time. Finally Section 4 summarises our conclusions.

3.2 Simulations

3.2.1 Description

In Chapter 2 we have performed a series of dissipationless N-body simulations of a single merger between a pre-existing disc galaxy and a satellite, in order to study the formation of thick discs in a context of disc heating. Among the main results presented in Chapter 2, we find that such mergers are able to produce thick discs that are both structurally and kinematically similar to those observed in the Milky Way and in external galaxies (see also Velázquez & White 1999, and references therein). Structurally, the simulated thick discs have larger scale-lengths compared to the initial disc and their scaleheights are 3–6 times larger with a clear dependence on the initial inclination of the decaying satellite. When compared to observations of the Galactic thick disc, the simulations seem to favour mergers with low/intermediate initial inclinations for the formation of this component, as suggested by the measured $\sigma_{\rm z}/\sigma_{\rm R}$ ratio (as determined by, e.g., Soubiran et al. 2003; Vallenari et al. 2006) and from the presence and amplitude of vertical gradients in the mean rotation (Girard et al. 2006; Ivezić et al. 2008).

These simulations are therefore a good starting point to study the detailed phase-space structure of the remnant system, and to establish if it is possible to dynamically distinguish stars from the pre-existing disc from those of the accreted satellite. Furthermore, they may also be used to develop indicators to test the validity of this particular formation scenario for the Galactic thick disc.

Below we summarise our suite of numerical simulations, but refer the interested reader to Chapter 2 for more details.

We have explored the following initial configurations for the merger: (i) the structure and kinematics of the primary disc resemble those of a) the present Milky Way ("z=0" experiments); or b) a disc at redshift one ("z=1") according to the model of Mo et al. (1998). The latter represents a likely formation epoch of the Galactic thick disc as suggested by the age of its stars (Edvardsson et al. 1993); (ii) two stellar morphologies for the satellite: spherical or discy; (iii) two total (and stellar) mass ratios between the infalling satellite and the host galaxy (10% and 20%); and (iv) three initial orbital inclinations of the satellites, in both prograde and retrograde directions with respect to the rotation of the host disc.

Both the host galaxy and the satellite are modelled self-consistently with both star and dark matter (DM) particles. The stellar component of the satellite has structure and kinematics that are consistent with the observed fundamental plane of dE+dSphs galaxies. The satellite is launched far away from the host disc (35–50 times the host disc scale-length, depending on the experiment) and has orbital parameters that are consistent with cosmological studies of infalling substructure (Benson 2005). We will use here the simulations of 20% mass ratio between the satellite and the host galaxy. This results in a sample of 24 simulated thick discs. The stellar components of the satellite and of the host disc are modelled with 10^5 particles, implying that the satellite's stars are over-represented in number (by a factor of five) in the merger remnant.

As a reference, Table 3.1 summarises both the structural and the kinematical properties of the final thick discs of Chapter 2. The kinematical properties listed here were measured at R=2.4$R_{\rm D}$ for both "z=0" and "z=1" experiments, corresponding to ∼11 kpc and ∼5 kpc, respectively. Between brackets we also quote these values for the "z=1" case at R=3.6$R_{\rm D}$, i.e. ∼8 kpc. In the rest of this Chapter we focus mainly on the "z=1" experiments, since the final stellar mass of the remnant system, $\sim 1.4 \times 10^{10} M_{\odot}$, is comparable to that estimated for the Galactic thick disc (e.g. Robin et al. 2007).

For completeness, here we briefly remind the reader of the properties of the Milky Way thick disc. The measured scalelength of the Galactic thick disc is comparable to that of the thin disc, i.e. in the range 2.8–4.5 kpc; and its exponential scale-height z_0=700–2000 pc (Larsen & Humphreys 2003; Jurić et al. 2008). Kinematically, the velocity ellipsoid of the thick disc in the solar neighbourhood is observed to be ($\sigma_{\rm R}$,σ_{ϕ},$\sigma_{\rm z}$) ∼(65,54,38) km s^{-1} (Chiba & Beers 2001; Vallenari et al. 2006; Veltz et al. 2008). Thick disc stars have a rotational lag of ∼30–50 km s^{-1} (Chiba & Beers 2000; Veltz et al. 2008).

A close look at Table 3.1 shows that none of our simulated thick discs reproduce exactly the properties of the thick disc of the Milky Way. An additional point to bear in mind is that the structure of the merger remnants is likely to change if a new thin disc is formed from freshly accreted gas, as generally envisioned in the models explored here (e.g. Freeman & Bland-Hawthorn 2002). However, even if the detailed properties differ, we believe that studies of the dynamical phase-space structure of our remnants should give us insight into what observables can be used for example, to distinguish in-situ stars from those that have been accreted.

Table 3.1: Properties of final thick discs produced in Chapter 2.

"z=0"	0°	30°	60°
$R_{\rm D}$	4.47	4.59	3.96
z_0	1.25	1.63	1.78
$\sigma_{\rm R}$	94.7	84.5	69.5
σ_ϕ	74.3	62.8	55.4
$\sigma_{\rm z}$	46.3	53.4	54.6
$\overline{v_\phi}$	119.6	122.1	150.3
"z=1"	0°	30°	60°
$R_{\rm D}$	2.26	2.28	2.04
z_0	0.64	0.82	0.85
$\sigma_{\rm R}$	85.7(64.8)	76.4(53.9)	55.4(47.8)
σ_ϕ	56.7(54.8)	53.9(44.8)	48.2(28.3)
$\sigma_{\rm z}$	36.8(20.9)	41.7(32.5)	41.8(42.6)
$\overline{v_\phi}$	96.1(117.3)	107.8(120.7)	122.7(133.7)

- Scale-lengths ($R_{\rm D}$) and scale-heights (z_0) in kpc. Radial ($\sigma_{\rm R}$), azimuthal (σ_ϕ) vertical ($\sigma_{\rm z}$) velocity dispersions and mean rotation ($\overline{v_\phi}$) in km s^{-1}.
- Kinematics are measured at $2.4R_{\rm D}$ for "z=0" and at $2.4R_{\rm D}$ ($3.6R_{\rm D}$) for "z=1" experiments.
- Only experiments with prograde spherical satellites with masses 20% of $M_{\rm disc,host}$ are listed.

3.2.2 Definition of local volumes

Our interest lies in determining the structure of phase-space of our merger remnants especially in small volumes which may resemble the Solar neighbourhood. This is motivated by our aim to eventually compare our predictions to observations, and because typically we only have (access to) full phase-space information for relatively nearby stars.

Given that the scalelengths of our simulated thick discs are $\sim 35\%$ smaller than what has been estimated for the Milky Way, it is not straightforward to decide which radius would correspond to the "Solar circle". This is why we explore the phase-space structure in volumes located at two different radii, namely $2.4R_{\rm D}$ ($\sim$5 kpc) and $3.6R_{\rm D}$ ($\sim$8 kpc), where $R_{\rm D}$ is the final thick-disc scalelength in our experiments (see Table 3.1).

To obtain phase-space information from particle samples inside such volumes for our simulated thick disc, we first define a Cartesian system with the origin in the centre of mass of the thick disc and the z-axis aligned with its rotational axis. The angular momentum vector points towards the galactic south pole ($-z$), hence the rotation is clockwise. We place four identical spherical volumes onto the disc plane defined as being perpendicular to the angular momentum vector. The centres of these spheres have coordinates ($+R_{\rm v}$,0,0), ($-R_{\rm v}$,0,0), (0,$+R_{\rm v}$,0) and (0,$-R_{\rm v}$,0). $R_{\rm v}$ is defined as either $2.4R_{\rm D}$ or $3.6R_{\rm D}$. We explore spheres of several sizes but, unless noted otherwise, the rest of the Chapter will refer to volumes of 2 kpc radius.

Fig. 3.1 illustrates the volumes' coverage of the final thick discs for the case of the

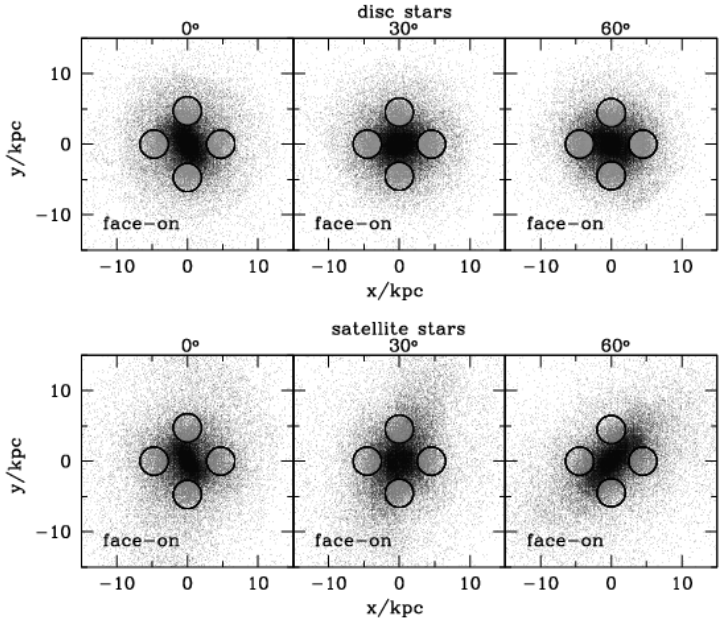

Figure 3.1: Coverage of the spherical volumes defined to analyse the phase-space structure of the simulated thick discs. The Figures show the final spatial distribution (in a face-on view) of "z=1" experiments with spherical satellites on prograde orbits for three different initial orbital inclinations. Volumes are centred at $R_{\rm v}$=2.4$R_{\rm D}$ ($\sim$5 kpc) from the galactic centre and are 2 kpc radius. Stars belonging to the heated disc (above) and to the satellites (below) are plotted separately to highlight the different spatial distributions.

"z=1" experiment using a prograde spherical satellite with initial inclination of 30°. The volumes are located at $R_{\rm v}$=2.4$R_{\rm D}$ from the galactic centre and are labelled from 1 to 4 according to where they are placed, i.e., $(+x,+y,-x,-y)\equiv(1,2,3,4)$.

In the next Section we will characterise the velocity distribution of stars in these local volumes. Because our remnant discs are not fully axisymmetric as evidenced in Fig. 3.1, it is important to establish first how the properties of the velocity distribution function depend on location. Therefore in Section 3.3.1 we quantify the deviations from axisymmetry and establish their impact on the velocity distribution. We then focus on the dynamical properties of the in-situ stars versus those accreted in Section 3.3.2 and Section 3.3.3.

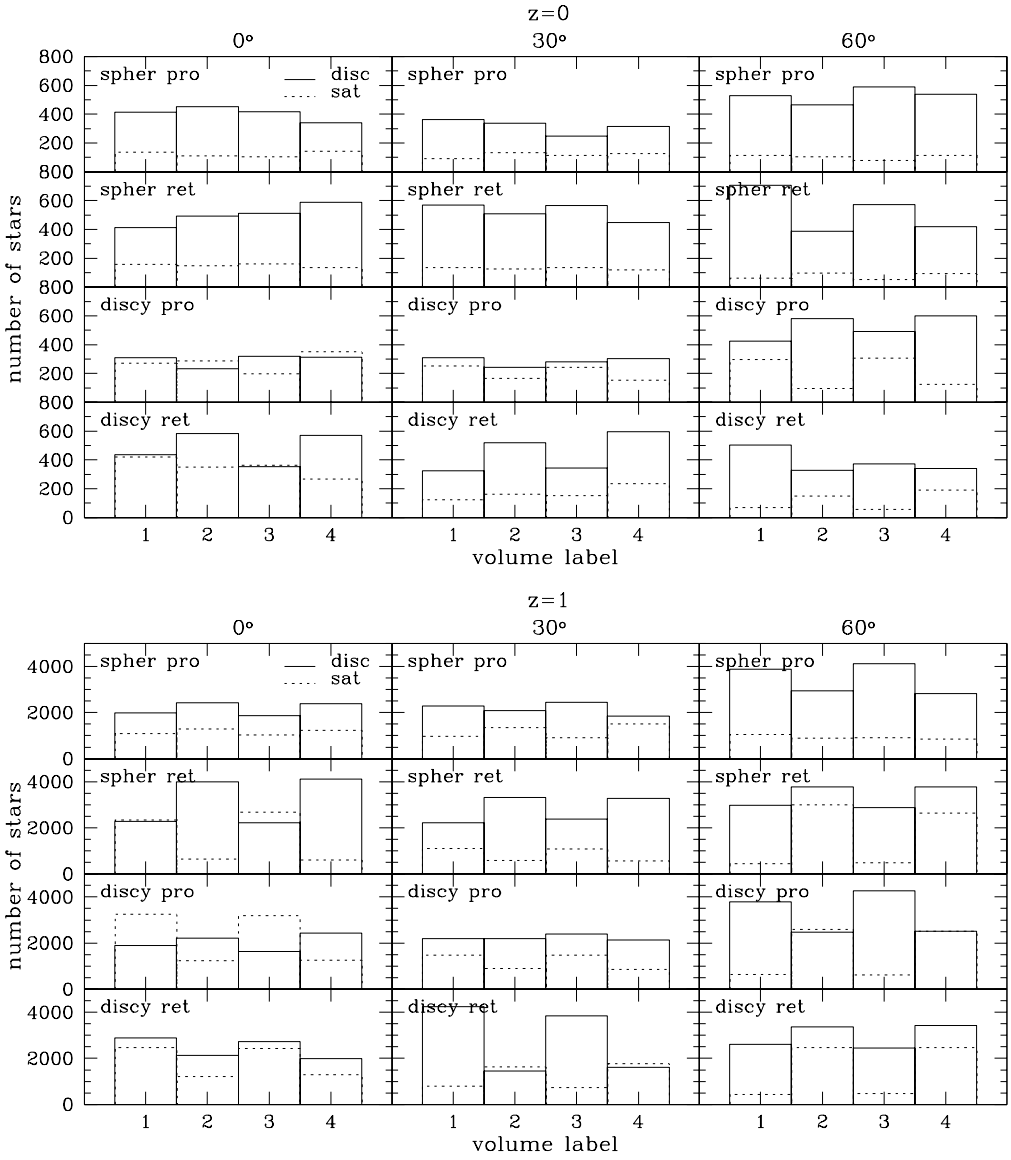

Figure 3.2: Number of disc and satellite stars within each volume for all the experiments at "z=0" and "z=1". The volumes are labelled from 1 to 4 according to their location on the xy plane ($+x$,$+y$,$-x$,$-y$, see Fig. 3.1). In general, the spatial distribution of stars is not uniform for all 4 volumes, indicating different degrees of deviation from axisymmetry in both the heated disc and the satellite debris.

3.3 Results

3.3.1 Effect of non-axisymmetries

On the spatial distribution

Fig. 3.1 shows that the distributions of heated disc particles and satellite particles are not symmetric with respect to the rotation axis of the system. Note that there does not seem to be a correlation in the deviations from axisymmetry between the disc and the satellite stars. This suggests that these asymmetries are likely to have different origin.

Fig. 3.2 gives a general overview, for all 24 of our experiments, of the distributions of stars in the final thick discs. This Figure shows the variation of the number of stars from volume to volume for each experiment. Note that, in order to facilitate the comparison, the number of satellite stars has not been normalised according to mass ratio between host disc and the stellar component of the satellite (see Chapter 2), meaning that they are over-represented by a factor of five. Overall, in each experiment, both disc and satellite present some degree of volume-to-volume alternation in the number of stars they contribute, demonstrating their asymmetric spatial distributions. In general, this alternation is different for the disc and for the satellite stars.

Fig. 3.3 shows the global amplitudes of the $m = 2$ deviations of both disc (left panels) and satellite (right panels) spatial distributions as a function of the initial orbital inclination of the satellites, for all 24 experiments. The amplitudes are measured by first binning the final spatial distributions of stars in cylindrical shells, within $|z| < 5$ kpc and $|z| < 3$ kpc for experiments at "z=0" and "z=1", respectively. Then for each bin the Fourier components of the second harmonic of the angular distribution are computed as:

$$a_2 = \frac{1}{N}\sum_{i=1}^{N}\sin(2\phi_i), \qquad b_2 = \frac{1}{N}\sum_{i=1}^{N}\cos(2\phi_i), \tag{3.1}$$

(Valenzuela & Klypin 2003 and references therein) with N the number of stars in each bin and ϕ_i the stars' angular position. For each bin the amplitude of the second harmonic is $A_2^2 = (a_2^2 + b_2^2)/2$. The global amplitude is then defined as $\langle A_2 \rangle = \sqrt{\langle A_2^2 \rangle}$, averaging over radii $R < 1.5R_{\rm D}$. Additionally, the angular phase of the $m = 2$ deviations are measured by finding the principal axes of the inertia tensors of the spatial distribution of stars projected onto the xy plane. In general, strong disc asymmetries are present out to a distance of ∼3–4 kpc ($\sim 1.7R_{\rm D}$) for the "z=1" experiments.

Fig. 3.3 shows that in general, for both disc and satellite stars, there are no clear dependencies of the $m = 2$ amplitude with inclination. However it is interesting to notice that discy satellites on retrograde orbits have induced the largest $m = 2$ deviations on the heated discs. This can be explained by the fact that this type of satellite loses mass faster as it evolves in comparison to spherical satellites (see Fig. 2.3 in Chapter 2). This results in a smaller drag force and hence in a longer decay timescale. Moreover, in general satellites on retrograde orbits are found to need more time to decay (see Fig. 2.2 in Chapter 2) which is a consequence of the weaker dynamical friction exerted by the main disc as compared to the prograde orbit case (see also Velázquez & White 1999). Therefore, the aforementioned satellite configuration induced a longer lasting and more powerful asymmetric perturbation on the main disc, eventually leading to the formation of a bar with a larger amplitude.

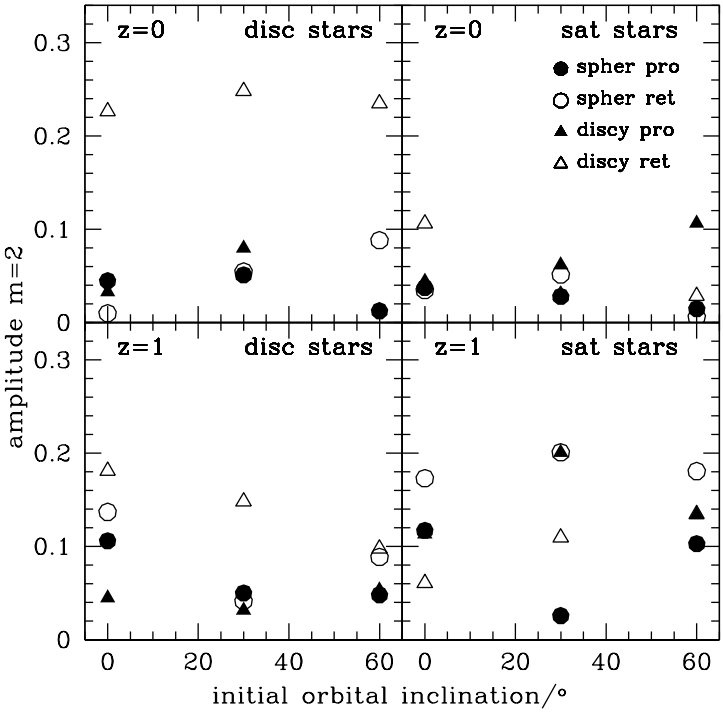

Figure 3.3: Global amplitudes of the $m = 2$ deviations from axisymmetry in the final spatial distributions of both disc (left panels) and satellite (right panels) stars for all experiments at "z=0" (upper panels) and "z=1" (lower panels).

On the other hand, the $m = 2$ deviations for the satellite debris seem to reach similar amplitude independently of the satellites' morphologies and initial orbital inclinations. This suggests that $m = 2$ deviations for disc and satellite stars may be caused by different dynamical effects. The satellites in our simulations have rather radial orbits (apo-to-peri ratios ~ 5, see also Section 2.3.1 in Chapter 2), for all initial orbital inclinations. This implies that their angular momenta are relatively low, or in other words that the amount of energy associated to tangential motions is much smaller than that associated to motion in the radial direction. This in turn, means that the precession rate of these orbits is slow. Furthermore, our satellites are relatively cold in comparison to the host galaxy. These factors make the range of orbital angular frequencies of satellite stars quite small, implying that that the mixing in the angular direction has to take place on fairly long timescales. Thus as the satellite gets disrupted, its stars remain somewhat constrained in azimuth, which results in the observed $m = 2$ deviations, in rather close analogy to what happens as a result of the radial orbit instability (Binney & Tremaine 2008).

There are two important implications of the characterisations made above. Firstly thick discs could well be asymmetric because of the presence of a small central bar. Secondly, the fraction of accreted stars may well vary with azimuthal angle in the plane

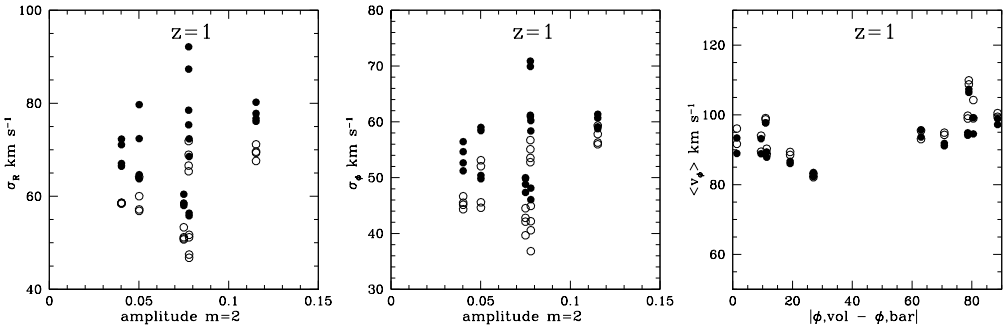

Figure 3.4: Radial (left panel) and tangential (central panel) velocity dispersions in each volume as a function of the amplitude of the $m = 2$ deviations from axisymmetry in the spatial distribution of disc stars for all prograde "z=1" experiments. Velocity dispersions are shown considering both disc and satellite stars (solid circles) and disc stars only (open circles). The panel on the right shows the mean rotational velocity in each volume as a function of the angular separation between the volume and the major axis of the "bar" formed by the disc stars, for all "z=1" experiments.

of the thick disc. In recent years, Parker et al. (2003, 2004) have found evidence that indeed the Galactic thick disc may be asymmetric. More recently, the suggestion has been made that the stellar asymmetry of faint thick-disc/inner-halo stars in the first quadrant ($l = 20^{\rm o} - 45^{\rm o}$) could be an indication of a triaxial thick disc or a merger remnant/stream (Larsen et al. 2008).

On the kinematics

In order to investigate the possible effects of the "bars" on the kinematics of stars in our local volumes, we have computed several statistical moments of the velocity distributions (mean, dispersion, skewness and kurtosis). We have then correlated these properties to both the location and the amplitude of the $m = 2$ deviations of the spatial distribution of disc stars (since this bar dominates in terms of mass/surface density as compared to the triaxial distribution of accreted stars which never dominate the central regions nor near the plane, see Chapter 2). In general, we do not find a significant dependence of the moments with respect to the strength of $m = 2$ deviations. This is shown explicitly in the left and central panels of Fig. 3.4, where we have plotted the radial and tangential velocity dispersions within each volume, for all prograde experiments at "z=1", as a function of the induced global $m = 2$ amplitudes. Note that similar results are obtained when the dispersions are computed considering either disc stars only (open circles) or disc and satellite stars jointly (solid circles). Only weak trends are found for the mean rotational velocity $\langle v_\phi \rangle$ when computed as a function of the relative location of the volume with respect to the position angle of the bar, as shown in the rightmost panel of Fig. 3.4. When the various moments are computed in volumes which are located farther away from the centre, such as at $3.6R_{\rm D}$, the correlations are even less prominent.

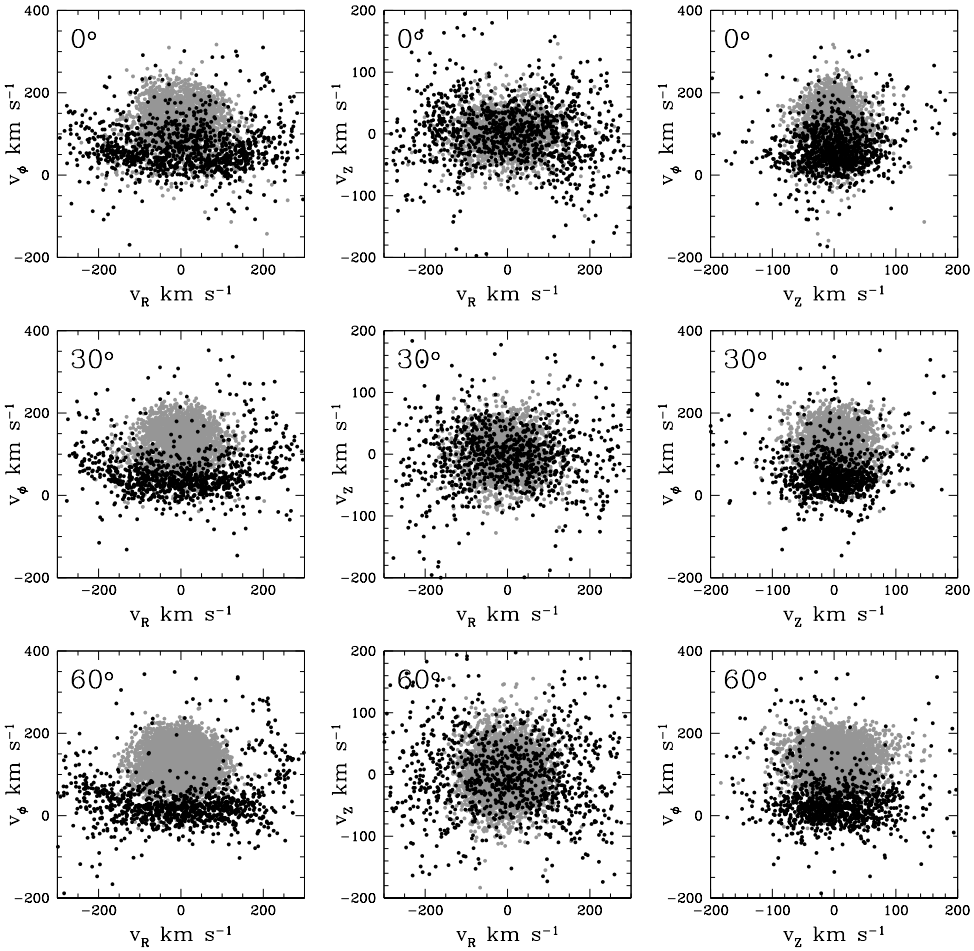

Figure 3.5: Final velocity distribution of disc (grey) and satellite (black) stars for different initial orbital inclinations of a prograde spherical satellite: 0°(upper row), 30° (middle) and 60° (bottom); corresponding to "z=1" experiments. Stars are within spheres of 2 kpc radius located at R=2.4$R_{\rm D}$ from the galactic centre. All satellite stellar particles have been plotted here, implying that they are over-represented by a factor of five.

3.3.2 The kinematics of disc and satellite stars

Fig. 3.5 shows the final velocity distributions of both disc (grey) and satellite (black) stars for the "z=1" experiments with a spherical satellite with initial inclinations of 0°, 30° and 60° on a prograde orbit. The stars plotted in this Figure are enclosed within a spherical volume centred at $R = 2.4R_{\rm D}$.

This Figure shows that disc and satellite stars have radically different distributions in velocity space. For instance, in the $v_{\rm R} - v_\phi$ plane, satellite stars are distributed in a banana-shape, whereas the disc stars define a centrally concentrated clump. This

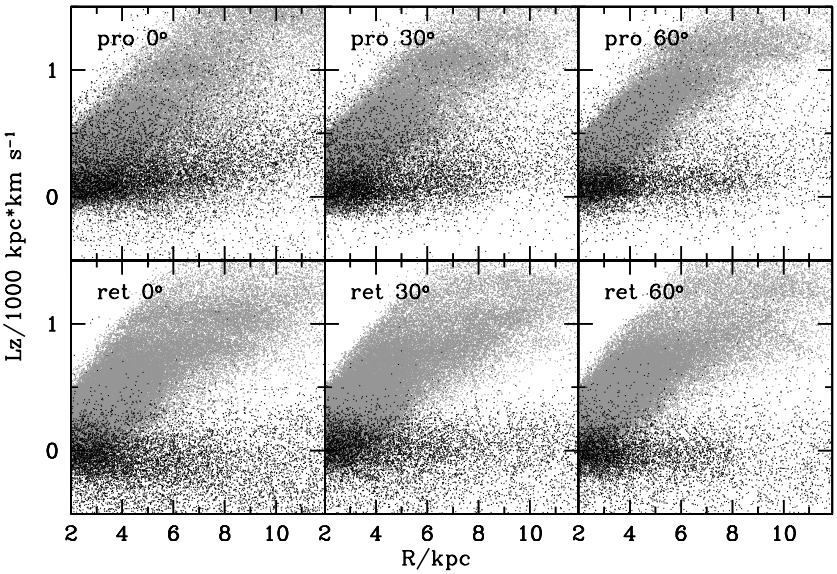

Figure 3.6: Final distribution of L_z of disc (grey) and satellite stars (black; only one in five is shown) as a function of galactic radius, for prograde (top row) and retrograde (bottom row) satellites with initial orbital inclinations 0° (first column), 30° (second) and 60° (third). Stars are located within $2 < R < 12$ kpc and $|z| < 1$ kpc.

difference is a consequence of the more eccentric orbits of the accreted stars compared to those from the disc. The accreted stars that cross the volume under consideration have slightly different orbital phases, i.e. stars with $v_{\rm R} = 0$ are at the apocentre while those travelling either towards (or away from) it have $v_{\rm R} > 0$ (or $v_{\rm R} < 0$), leading to this very characteristic banana-shape (see also Helmi & White 1999b). In the $v_{\rm R} - v_{\rm z}$ plane satellite stars populate mostly the outskirts of the distributions, with a clear dependence on the initial orbital inclination. Stars from the satellites on more inclined orbits show larger vertical velocities as they cross the disc plane as expected. Both the $v_{\rm R}$ and $v_{\rm z}$ distributions are very symmetric, showing that the stellar particles are well mixed in these directions by the end of the simulation. Satellite stars typically have lower mean rotational velocity in comparison to disc stars, as can be seen in the $v_{\rm z} - v_\phi$ plane.

In Fig. 3.6 we show the final distributions of the z-component of the angular momentum (L_z) of both disc and satellite stars as a function of cylindrical radius, for "z=1" experiments with a discy satellite. In this Figure, stars are located within $2 < R < 12$ kpc and $|z| < 1$ kpc. The trend followed by the disc stars reflects a constant rotational velocity (hence $L_z \propto R$). The stars from the satellite, on the other hand, do not show this same trend, since their z-angular momenta are relatively constant with radius; the absolute value being related to the initial conditions of the satellite's orbit. This is why the separation between both types of stars has a mild trend with initial orbital inclination of the satellite, especially for prograde orbits, and also why the retrograde cases have

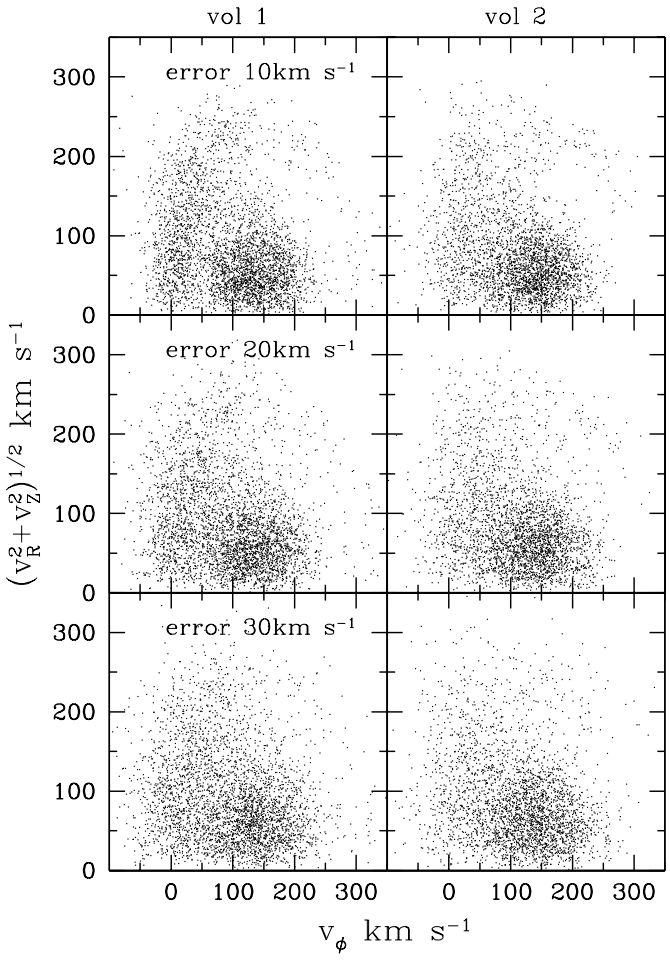

Figure 3.7: Toomre diagrams of "z=1" experiments for prograde discy satellites with initial orbital inclination 30° after convolution of each velocity component with a Gaussian error of: 10 (upper row), 20 (middle) and 30 (bottom) km s^{-1}. In the case of errors $\sim$10 km s^{-1}, disc and satellite stars are easily distinguishable (disc stars have $\overline{v_\phi} \sim 120$ km s^{-1}). Volumes 1 and 2 are shown to illustrate the difference in the distribution of stars due to the $m = 2$ deviations from axisymmetry in the spatial distributions of disc and satellite stars. Satellite particles are overrepresented in this Figure by a factor of five.

negative $\langle L_z \rangle$. This Figure suggests that in order to distinguish more easily between disc and satellite stars, it is better to study the kinematics at large galactocentric distances.

Note that these conclusions can be generalised rather easily, and are quite independent of the particular initial configuration of the merger. For example, an increase in the initial tangential velocity of the satellite, will lead to a higher final value of L_z, implying that the distinction between accreted and in-situ stars will be more difficult near the Sun. In such cases, one would have to compile samples of stars located at much larger distances in the plane, such that the final L_z distribution at this location would be bimodal, as seen for example, at $R \sim 8$ kpc in Fig. 3.6.

It is also important to stress here that the trend of L_z as function of R observed for the stars in the heated disc, constitutes a rather clean test of the formation scenario for the Galactic thick disc studied here. Such a trend would be expected only in the case a pre-existing thin disc was present at early times, since only then most of the stars would be moving on nearly circular orbits.

Fig. 3.7 shows the Toomre diagrams for the "z=1" experiment with a prograde discy satellite with initial inclination 30º, including disc and satellite stars. Note that the satellite particles are over-represented in this Figure by a factor five. The three velocity components have been convolved with Gaussian errors of 10, 20 and 30 km s^{-1}. The volumes contain different number of particles due to the asymmetric spatial distributions discussed in Section 3.3.1. The separation between both types of stars is evident even if the errors in the velocity are 20 km s^{-1} and should allow the distinction between satellite stars and heated disc stars in surveys such as RAVE (Steinmetz et al. 2006).

3.3.3 Statistical tests on the velocity distributions

KS test on the $v_{\rm R}$, v_ϕ and $v_{\rm z}$ distributions

As just discussed, significant merger events like those simulated in Chapter 2 leave clear and long-lasting signatures in the kinematics of the final systems. Fig. 3.5 shows that disc and satellite stars clearly dominate different regions of velocity space, and that the final distributions are not Gaussian. In this section we quantify this non-Gaussianity, by studying the 1-dimensional velocity distributions along the R, ϕ and z directions in our local volumes. To this end we perform the Kolmogorov-Smirnov/Kuiper* statistical test (e.g., see Press et al. 1992). Our null hypothesis is that the underlying velocity distributions are Gaussian along each one of the principal axes of the velocity ellipsoid ($v_{\rm R}$, v_ϕ, $v_{\rm z}$).

Fig. 3.8 shows the disc+satellite velocity distributions of $v_{\rm R}$ and v_ϕ and the best Gaussian fit (dashed lines) for a "z=1" experiment with a prograde discy satellite with initial orbital inclination 30º. The stars considered here are located in volumes of 2 kpc radius at $R = 2.4R_{\rm D}$ and $R = 3.6R_{\rm D}$ (left and right panels, respectively), and the number of satellite stars has been properly normalised (effectively, only 1 in 5 stars is considered). This Figure shows that in most cases our null hypothesis can be rejected with better than 3σ confidence. This is mainly because the simulated velocity distributions have rather extended wings. These wings are preferentially dominated by satellite stars, also in the case of the $v_{\rm z}$ distributions (see Fig. 3.5). However, in this latter case the contribution of satellite stars to the wings is too low (by number) to be detected by the test. As expected (Section 3.3.1) the results of this test are nearly independent of the azimuthal location of the volumes. Note that even in these small samples, the features are very significant, and should be relatively easy to detect observationally. Furthermore, the velocity distributions do bear a close resemblance to those seen in the in-situ samples studied by Gilmore et al. (2002b).

Heliocentric line-of-sight velocities, $v_{\rm los}$

In practice, it is relatively difficult to obtain accurate full space velocities for large samples of stars. The main challenge being to measure accurately their proper motions and distances for the stars. However, a possible workaround to this problem is to concentrate on heliocentric line-of-sight velocities ($v_{\rm los}$) which are comparatively cheaper to obtain and can be measured with high accuracy for large samples of stars.

* The Kuiper variant of the test is chosen instead of the standard Kolmogorov-Smirnov since the first guarantees equal sensitivity at all values of the distribution, particularly in the wings.

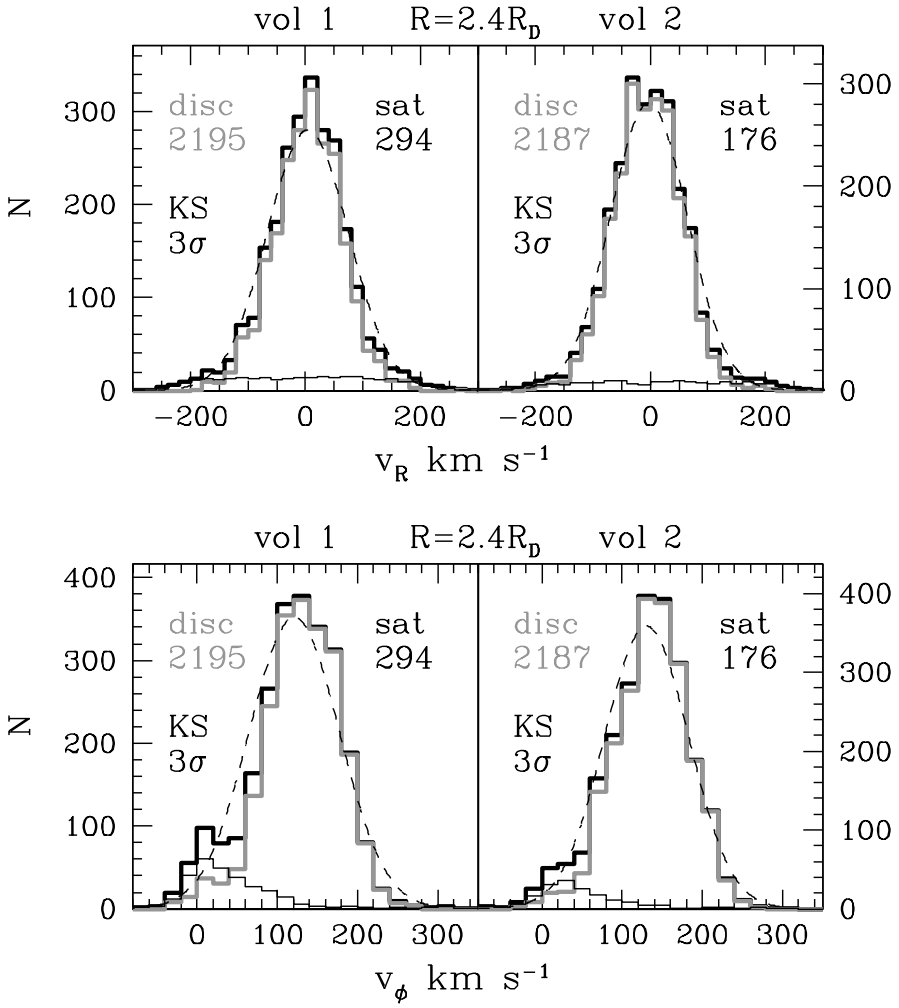

Figure 3.8: Histograms of the radial (top) and tangential (bottom) velocities of stars within volumes centred at $R = 2.4R_{\rm D}$ and $R = 3.6R_{\rm D}$, for "z=1" experiments with a prograde discy satellite with initial orbital inclination 30°. KS/Kuiper tests have been performed in order to obtain a probability that the total distribution of stars (thick black line) is drawn from a Gaussian distribution (obtained as the best fit to the total distribution). Distributions of disc (grey line) and satellite (thin-black line) stars are also shown. The labels "KS 3σ, 2σ or '$\times$' (meaning less than 1σ)" indicate the confidence level with which one can establish that the distribution has not been drawn from the best fit Gaussian. Volumes 1 and 2 are shown to illustrate the difference in the distributions due to asymmetric spatial distributions of disc and satellite stars. *(Continues on next page)*

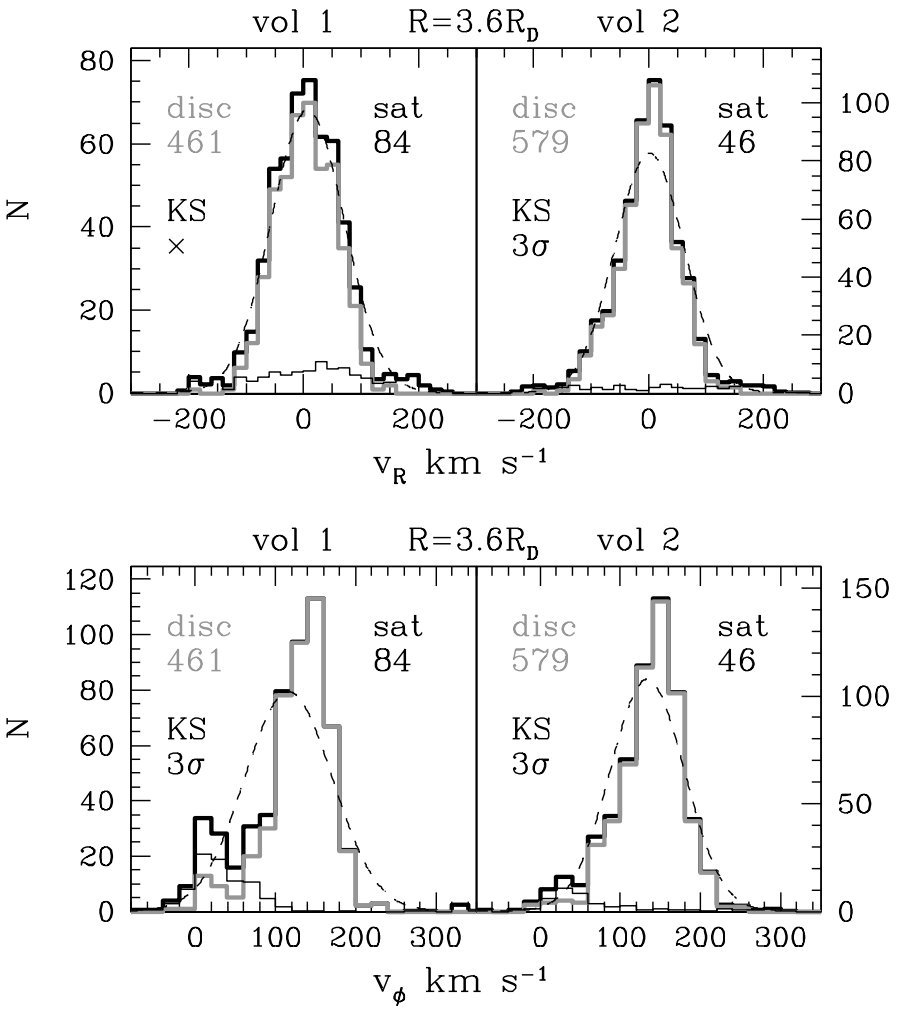

Figure 3.8: *Continuation.*

In our simulations we compute the $v_{\rm los}$ as follows. First both the galactic longitude (l) and latitude (b) are computed for each star with respect to the centre of the local volume, with the $+x$-axis pointing towards the galactic centre and the $+y$-axis in the sense of rotation of the system. Then $v_{\rm los}$ is computed as:

$$v_{\rm los} = v_{\rm x} \cos l \cos b + v_{\rm y} \sin l \cos b + v_{\rm z} \sin b \tag{3.2}$$

where the three velocity components of each star are measured with respect to the galactic centre (i.e. they include the galactic rotation). This implies that stars on circular low latitude orbits have $v_{\rm los} \sim v_{\rm circ} \sin l \cos b$, since $v_{\rm x}$ and $v_{\rm z}$ should both be (close to) zero.

The upper panels of Fig. 3.9 show the $v_{\rm los}$ of disc (grey) and satellite (black) stars as

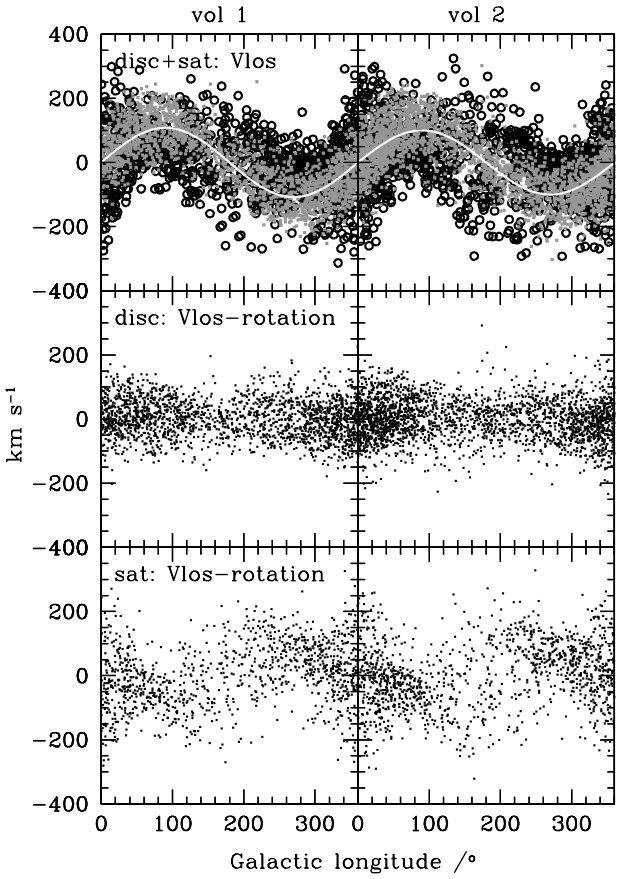

Figure 3.9: *Top panels*: Heliocentric line-of-sight velocities of disc (grey) and satellite (black) stars. The white line shows a $\sin(l)$ fit to model the mean rotational velocity of the final thick disc. *Middle and bottom panels*: The rotation signal has been subtracted for both disc and satellite stars, respectively. The Figures correspond to the "z=1" experiment using a prograde spherical satellite with initial orbital inclination 30°. Volumes 1 and 2 are shown to illustrate the difference in the distributions due to asymmetric spatial distributions of disc and satellite stars. In all the panels, the satellite stars are over-represented by a factor five.

a function of their galactic longitude for the "z=1" experiment with a prograde spherical satellite with initial orbital inclination of 30°. The most evident feature is that stars of the heated disc are still rotating on fairly circular orbits in spite of the relatively massive minor merger, as demonstrated by the sinusoidal dependence on galactic longitude of their line-of-sight velocities.

We proceed to subtract the mean rotation of the system, $v_{\rm rot}$, in order to better quantify the contribution of the satellite stars to the wings of the distributions of $v_{\rm los}$. The mean rotation is found by fitting to the $v_{\rm los}(l)$ distribution of both disc and satellite stars (after the proper normalisation) the one-parameter function $v_{\rm rot}\sin(l)$. The result is the white curve in the top panel of Fig. 3.9. The middle and bottom panels of this Figure show both disc and stars radial velocities obtained after subtracting $v_{\rm rot}$. The different behaviour of disc and satellite stars is very clear now, and this is also the case for most of our experiments. In the particular example plotted here, the maximum separation is found around $l \sim$100–160° and $l \sim$220–240° as illustrated in the Figure. Note finally that the $m = 2$ deviations from axisymmetry do not significantly impact the distributions, i.e. there are no large volume-to-volume differences.

In Fig. 3.10 we have plotted the $v_{\rm los}$ distributions of disc+satellite stars, after sub-

tracting $v_{\rm rot}$, for all "z=1" experiments with spherical satellites. The stars included in the histograms have galactic longitudes within an interval of $\delta l = 40^{\rm o}$ around $l = 140^{\rm o}$ (where the difference between the two populations of stars was largest according to the previous Figure). At these longitudes, $l \sim 140^{\rm o}$, most of the satellite stars have negative $v_{\rm los}$. This is manifested in most of the distributions shown in Fig. 3.10, which are (slightly) asymmetric and tend to have a prominent negative velocity tail, particularly compared to the best fit Gaussian (denoted here by the dashed curves). To further emphasise this point, the open circles in Fig. 3.10 denote the fraction of satellite stars present at a given velocity (bin).

We quantify the statistical significance of the features present in the $v_{\rm los}$ distributions by computing a probability that measures the likelihood of the "observed" number of stars in a given velocity bin. We proceed as follows. We first generate $N_{\rm tot,real} = 10^4$ random realisations based on the best Gaussian fit. We then define the probability of observing $N_{{\rm obs},i}$ stars or more in the i-th bin as:

$$P_i(\geq N_{{\rm obs},i}) = \frac{N_{\rm real}(N_{{\rm gen},i} \geq N_{{\rm obs},i})}{N_{\rm tot,real}}, \tag{3.3}$$

where $N_{{\rm gen},i}$ denotes the number of "random stars" present in the i-th bin. Therefore the numerator in Eq. (3.3) denotes the number of realisations for which the number of "random stars" is greater or equal the observed one for each bin.

The resulting probabilities $P_i(\geq N_{{\rm obs},i})$ are depicted as the solid circles in Fig. 3.10. Typically very low probabilities ($< 1\%$) are obtained in the wings of the velocity distribution, as well as near the central peak. Recall that the wings are dominated by satellite stars (as indicated by the open circles). This implies that this test is both able to identify non-Gaussian features, as well as the presence of accreted stars. The low probabilities found near the central peak are due to the fact that this region is dominated by stars in a cold remnant disc, which survives the merger event, and contains $10-20\%$ of the total mass of the thick disc (see Section 3.4 of Chapter 2).

Similar results are found for all our experiments (also those not shown in Fig. 3.10). In general, after analysing similar histograms for all the experiments, we find that even when the histograms contain a relatively small number of stars, it is possible to detect rare peaks in the wings which are composed mostly by satellite stars.

At this point it is important to remind the reader that the simulations performed in Chapter 2 do not include the growth of a fresh thin disc after the merger that led to the formation of the thick disc. This new, colder and (presumably) more massive thin disc would *mostly* dominate around $v_{\rm R} \sim 0$ and $v_{\rm z} \sim 0$ km s^{-1}. For example, in Fig. 3.8 it should result in an enhancement of the central peak of the $v_{\rm R}$ and v_z distributions. On the other hand, in the direction of rotation a pronounced peak should be present at $\overline{v_\phi}_{,\rm thin}$, where $\overline{v_\phi}_{,\rm thin} > \overline{v_\phi}_{,\rm thick}$. This implies that the satellite stars are expected to remain the main contributors to the wings of all the velocity distributions. The deposition of a significant amount of mass in the galactic plane should lead to an increase in the rotational velocity of the thick disc stars, and hence the line-of-sight velocities should still show a sinusoidal dependence on longitude, but now with a larger amplitude than that visible in Fig. 3.9. Satellite stars will continue to dominate the wings of the $v_{\rm los}$ distributions and should clearly become apparent after the mean rotation of disc has been subtracted.

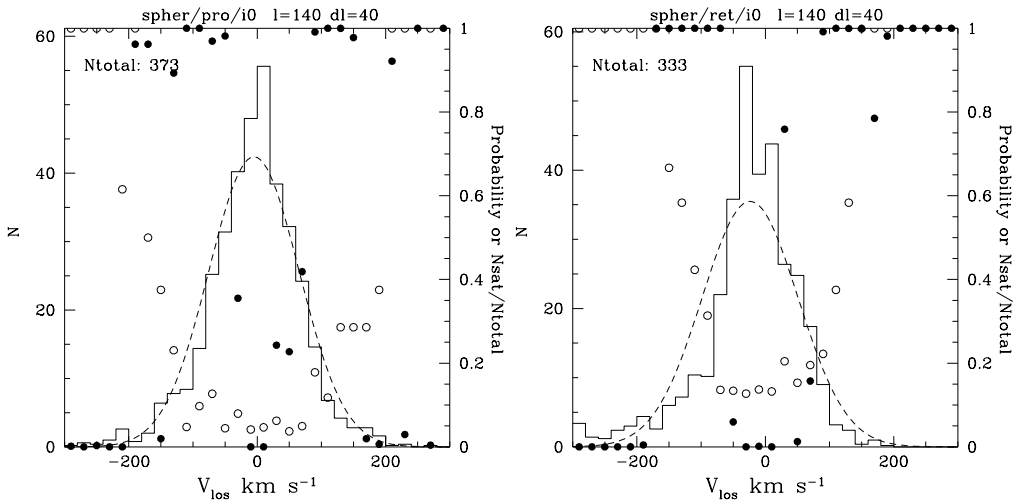

Figure 3.10: Histograms of the heliocentric line-of-sight velocities after subtracting the mean rotation of the final thick disc, for "z=1" experiments using prograde and retrograde spherical satellites with initial orbital inclinations of 0°, 30° and 60°. The histograms include disc and satellite stars within a slice around l ∼140°, where the contribution of satellite stars to the wings is maximal (see Fig. 3.9). The width of l-slices is 40°. The best Gaussian fits to the histograms are shown in dashed. The open circles show the fraction of satellite stars in each velocity bin. The solid circles denote the probability of the observed number of stars compared to what is expected from the best fit Gaussian at each velocity bin. *(Continues on next page)*

3.4 Summary and Conclusions

In this follow-up study we have analysed the phase-space properties of a sample of 24 simulated thick discs presented in Chapter 2. These thick discs have been produced via a significant merger between a pre-existing disc galaxy and a satellite. In that study several combinations of the initial conditions of the progenitors were explored, such as: two redshifts of formation ("z=0" and "z=1"); two mass ratios between the main disc galaxy and the satellite (10% and 20%); two different morphologies for the stellar component of the satellite (spherical and discy); and three initial orbital inclination of the satellites (0°, 30° and 60°) in both prograde and retrograde orbits.

The goal of this Chapter has been to find robust indicators of the merger origin of these simulated thick discs by characterising their phase-space structure. This involves establishing which properties from the progenitors have been retained in the final system as well as ways to distinguish dynamically in-situ and accreted stars. Our ultimate goal is to shed light onto the origin of the thick disc of the Milky Way by comparing the predictions of this model to already available (and future) surveys of nearby stars such as RAVE, SEGUE and *Gaia*.

Our simulations show that the final spatial distributions of stars from both the heated disc and satellite are usually asymmetric with respect to the rotation axis of the system,

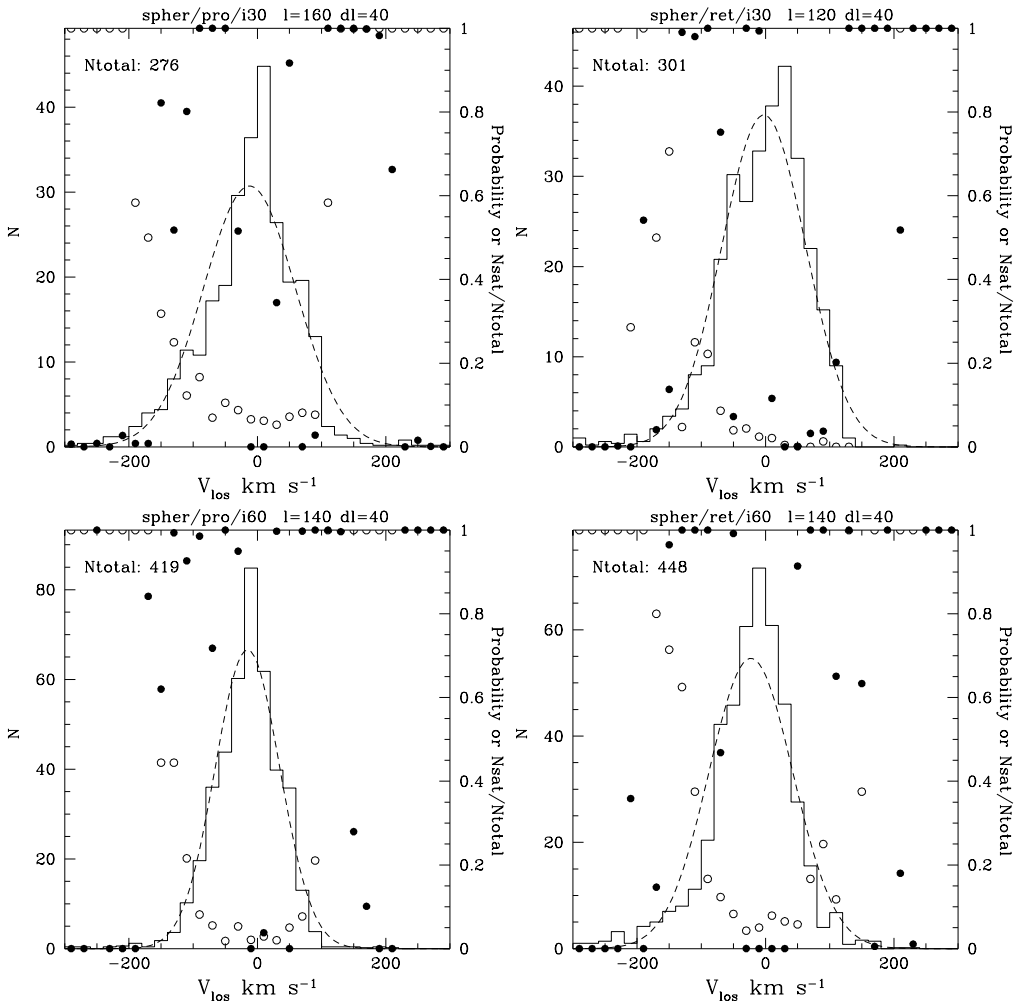

Figure 3.10: *Continuation.*

but that each of these "$m = 2$" deviations are generally out of phase. The lack of apparent correlation between these asymmetries suggests that they could originate in different dynamical processes. Indeed, the "bar-like" distribution of heated disc stars seems to be induced by the asymmetric perturbation of the decaying intruder, while the asymmetry in the distribution of satellite stars bears some analogy to the radial orbit instability. It is interesting to notice that similar spatially asymmetric distributions have been observed in the thick disc of the Milky Way (e.g. Larsen et al. 2008). In terms of kinematics, these asymmetries are found to have a negligible effect on the velocity distributions of both heated disc and satellite stars.

When samples of thick disc stars are selected in small volumes that resemble "solar neighbourhoods", we find clear differences in the velocity distributions of in-situ and

accreted stars. The stars from the heated disc are more centrally concentrated in $v_{\rm R}$ and $v_{\rm z}$ while the accreted stars show broader velocity distributions in these directions. Additionally, the accreted stars rotate more slowly and they show a characteristic "banana-shaped" distribution on the $v_{\rm R} - v_\phi$ plane. It is important to note that similar features are observed independently of the size and location of the volumes on the midplane.

The vertical component of the angular momentum, L_z, as function of distance from the galaxy's centre is found to be a clear discriminator to separate heated disc stars from those accreted. In all our experiments in-situ stars have $L_z \propto R$ whereas for accreted stars L_z is approximately constant (i.e. independent of R). This implies that the distribution of L_z is predicted to be bimodal, and that the bimodal nature should become more apparent with increasing distance from the galactic centre. The $L_z \propto R$ behaviour thus provides a clean test of the presence of a pre-existing disc from which the Galactic thick disc stems. Note that such a behaviour would also be expected if the thick disc would have resulted from resonant interactions with transient spiral arms as proposed by Roškar et al. (2008). In this case, however, one would not expect to find a second component associated to the accreted satellite.

We also find that heliocentric line-of-sight velocities ($v_{\rm los}$) as a function of galactic longitude show that most heated disc stars remain on nearly circular orbits. This implies that even after a significant merger, the heated disc is able to retain part of the dynamical characteristics of the pre-existing disc (namely the relatively low orbital eccentricities). After subtracting the mean rotation, the wings of the $v_{\rm los}$ distributions are found to contain mostly accreted stars. Our analysis shows that the contribution of accreted stars to the wings is statistically measurable and, in principle, it could be easily detected surveys in the solar neighbourhood.

Finally, it is important to highlight the robustness of the results presented in this Chapter regarding the different initial conditions explored. For instance, the significant separation between heated disc stars and satellite stars in terms of L_z as a function of galactic radius. Even though the separation shows a mild trend with the satellite's initial orbital inclination, in all cases the separation is clear, especially when stars are located at large galactocentric radii. Similarly, the sinusoidal behaviour of $v_{\rm los}(l)$ is observed in all experiments independently of the size or location of the volumes. The robustness of these results allow us to consider them as direct probes of the disc heating scenario for the formation of thick discs. We aim to soon test these predictions on surveys of nearby stars such as RAVE to shed light on the formation of the Galactic thick disc.

Acknowledgements

We acknowledge financial support from the Netherlands Organisation for Scientific Research (NWO). The simulations were run in the Linux cluster at the Centre for High Performance Computing and Visualisation (HPC/V) of the University of Groningen in The Netherlands.